Journal of Materials Chemistry B

ROYAL SOCIETY OF CHEMISTRY

PAPER

View Article Online
View Journal | View Issue



Cite this: J. Mater. Chem. B, 2020, 8, 10586

# A benzothiazolium-based fluorescent probe with ideal p$K_a$ for mitochondrial pH imaging and cancer cell differentiation†

Bo Lin,[a] Li Fan,[a] Ying Zhou,[a] Jinyin Ge,[a] Xueli Wang,[b] Chuan Dong,[a] Shaomin Shuang *[a] and Man Shing Wong *[b]

Received 15th May 2020,
Accepted 27th September 2020

DOI: 10.1039/d0tb01253j

rsc.li/materials-b

A mitochondrial pH sensing fluorescent probe namely 2-(2-(6-hydroxynaphthalen-2-yl)vinyl)-3-(6-(triphenylphosphonio)hexyl)benzothiazol-3-ium bromide (**HTBT2**) was designed and facilely synthesized *via* the Knoevenagel condensation reaction. **HTBT2** displayed a linear fluorescence enhancement at 612 nm in response to pH changes between 8.70 and 7.20. The p$K_a$ value was determined to be 8.04 ± 0.02, which might be ideal for mitochondrial pH ($pH_{mito}$ ~8.0) detection. **HTBT2** also exhibited a remarkable large Stokes shift of 176 nm, which could diminish the interference of excitation light. The results of live cell imaging studies suggested that **HTBT2** showed excellent targeting ability for mitochondria. Importantly, it was successfully applied to visualize mitochondrial pH changes in live cells and differentiate the $pH_{mito}$ difference between cancer cell lines and normal cell lines. Our results consistently supported that **HTBT2** held practical promise for the investigation of physiological processes related to $pH_{mito}$ changes and clinical potential for cancer cell differentiation.



## Introduction

Various complex physiological processes in eukaryotic cells can be implemented through a high level of compartmentalization *via* independent division and/or close cooperation between subcellular organelles. Compartmentalization is regarded as the result of evolving to provide distinct environmental conditions for matching the requirements from the optimal individual metabolic process, and to store energy *via* electromotive force between inside and outside the membrane.[1] Each organelle with different function requires a specific physiological pH condition to facilitate its metabolic process. For instance, lysosome with pH 4.5–5.0, Golgi with pH 6.0–6.7 and endosome with pH 5.5–6.5 are typical acidic organelles; the pH of the cytoplasm (6.8–7.2) and endoplasmic reticulum (~7.2) is nearly neutral.[2–5] However, the mitochondria pH ($pH_{mito}$) environment is markedly alkaline (~8.0) in resting cells resulting from proton ($H^+$) extrusion in the process of the respiratory electron transport chain reaction.[2–4,6] It is noted that information transmission, $Na^+/K^+/Ca^{2+}$ exchange and homeostasis, reactive oxygen species (ROS) production and bioenergy are closely related to $pH_{mito}$.[4,7] In particular, mitochondrial autophagy (mitophagy) and apoptosis are often associated with the acidification of mitochondria.[6,8,9] Moreover, some reports indicated that various pathological conditions are closely related to abnormal levels of mitophagy, for instance, neurodegenerative diseases, cardiovascular diseases, Parkinson's disease, Reye's syndrome and Alzheimer's disease.[8,10,11] Consequently, a reliable and accurate method for monitoring $pH_{mito}$ fluctuation *in situ* holds promise to elucidate mitochondria related physiology and diseases.

Fluorescent probes, particularly small molecular probes, have recently attracted great attention in bioanalysis and real-time bioimaging technologies in the imaging of live cells and organisms due to their excellent sensitivity and high spatial and temporal resolution. Cationic molecular probes have been found to be desirable for targeting mitochondria because the mitochondrial inner membrane potential is negative.[2–4,6,12] Tang *et al.*[13] reported the first mitochondrial pH molecular probe (spring red, p$K_a$ = 6.3) based on the quaternary ammonium ion as a targeting group and tertiary amines as a pH responsive site, which provided a new strategy for the mitochondrial pH

[a] College of Chemistry and Chemical Engineering, Shanxi University, Taiyuan, 030006, China. E-mail: smshuang@sxu.edu.cn; Fax: +86-351-7018842; Tel: +86-351-7018842

[b] Department of Chemistry and Institute of Advanced Materials, Hong Kong Baptist University, Hong Kong Special Administrative Region, China. E-mail: mswong@hkbu.edu.hk

† Electronic supplementary information (ESI) available: These data include experimental procedures; synthetic scheme, excitation and emission spectrum; mass and $^1H$ NMR spectra assays, fluorescence lifetime, selectivity, photostability, reversibility and MTT assay of **HTBT2**; dynamic experiments of **HTBT2** in SMMC-7721 cells, BEAS-2B cells and pc-12 cells; and fluorescence images of **HTBT2** stained SMMC-7721 cells after being treated with $H_2O_2$, PBS and NAC. See DOI: 10.1039/d0tb01253j

measurement. Subsequently, various mitochondrial pH fluorescent probes using tertiary amines to respond to the pH alterations have been developed successively.[10,14–17] However, the p$K_a$ values of these probes are far from ideal for $pH_{mito}$ ($\sim$8.0) measurement because tertiary amines are only sensitive to pH variations in an acidic environment, which poses a sensitivity issue. Song *et al.*[18] synthesized a fluorescein probe with a carboxyl group as a sensing site to respond to the pH changes for $pH_{mito}$ detection; nevertheless, the p$K_a$ (5.77 $\pm$ 0.03) of this probe is far from satisfactory. To improve sensitivity, Qi *et al.*[19–23] prepared fluorescein or rhodamine-based probes by introducing cycloimide as a pH responsive group, which raised the p$K_a$ of the probe close to the neutral range. By employing the phenolic hydroxyl groups as a $pH_{mito}$-sensing group, several $pH_{mito}$ probes with higher fluorescence yield and wider monitoring range have been reported.[6,24–29] The p$K_a$ values of these probes respectively were 5.88,[24] 6.79,[26] 8.85,[25] 7.33,[27] 7.33,[28] and 7.25,[29] which were far away from mitochondrial pH. Very recently, Zhang's group[30] and Wu's group[31] reported two probes utilizing tertiary amines and phenolic hydroxyl groups as pH-sensitive sites, respectively. However, these p$K_a$ values were still much lower than mitochondrial pH. Fortunately, Sarkar *et al.*[6] reported a 2-naphthol-derived probe, namely **CMP1**, exhibiting a p$K_a$ value of 7.86 $\pm$ 0.05 in living cells. Furthermore, $pH_{mito}$ changes in living cells introduced by carbonyl cyanide *m*-chlorophenyl hydrazone treatment were successfully observed with CMP1. However, to date, very few pH fluorescent probes with an ideal p$K_a$ value ($\sim$8.0) for mitochondrial imaging in live cells have been reported.

Benzothiazole dyes have been extensively used as various fluorescent probes due to their excellent optical performance, such as excellent photostability, large molar extinction coefficients and Stokes shift. Recently, we have constructed a ratiometric pH fluorescent probe (**BTNO**) by conjugated double bond bridged benzothiazole and binaphthol.[32] **BTNO** displays a p$K_a$ (7.91 $\pm$ 0.03) nearing mitochondrial pH, which was attributed to the use of phenolic hydroxyl groups as the pH sensitive group. Unfortunately, **BTNO** cannot be used to specifically detect mitochondrial pH because its structure did not contain the mitochondrial targeting group. Herein, we designed and synthesized a novel biocompatible fluorescent probe **HTBT2** (Scheme 1) by introducing triphenylphosphonium (TPP) as a mitochondrial targeting unit into compound **BTNO**. Besides, owing to the enhanced intramolecular charge transfer (ICT) process from the naphthol functionality to benzothiazolium, **HTBT2** exhibits a larger Stokes shift and longer emission wavelength compared with **BTNO**. Under neutral and acidic conditions, **HTBT2** emits a strong orange-red fluorescence, while under alkaline conditions, naphthoxide (**TBT**) was formed *via* the deprotonation of the hydroxyl group, then the ICT process and the fluorescence quenched due to the conversion of naphthoxide to naphthoquinone (**OBT**), in which charge separation in the conjugate structure is hardly stable. The fluorescence intensities of **HTBT2** at 612 nm and pH values exhibited a linear relationship in the range from pH 8.70 to 7.20. Its p$K_a$ value was found to be 8.04 $\pm$ 0.02, which matched well with mitochondrial pH ($pH_{mito}$ $\sim$8.0). Importantly, **HTBT2** showed potential to detect the $pH_{mito}$ fluctuations in live cells and differentiate the $pH_{mito}$ differences between cancer cells and normal cells. These results consistently suggested that **HTBT2** could be practically effective to investigate physiological processes associated with $pH_{mito}$ alterations.

## Results and discussion

### Effect of pH on spectroscopic properties of HTBT2

The pH-dependent absorption properties of **HTBT2** were investigated in the DMSO/Tris–HCl buffer (1/2, v/v) system under different pH conditions. As depicted in Fig. 1a, **HTBT2** exhibited a strong absorption band around 566 nm ($\varepsilon_1$ = 2583 L mol$^{-1}$ cm$^{-1}$) at pH 9.30. Upon decreasing pH from 9.30 to 6.40, the absorption band blue-shifted progressively from 566 nm to 436 nm ($\varepsilon_2$ = 2647 L mol$^{-1}$ cm$^{-1}$), giving rise to a well-defined isosbestic point at 479 nm. Concomitantly, the colour of the solution changed from yellow to yellow-green. Such a blue-shift phenomenon was attributed to the weaker π-electron delocalization in the protonated state of **HTBT2**. It should be noted that the peak at 556 nm still existed when the pH value was 3.0, which could be attributed to the ionization of **HTBT2** (Fig. S2, ESI†).

The fluorescence spectra of **HTBT2** at pH 6.40 (Fig. S1, ESI†) indicated that the excitation and emission maxima of **HTBT2** are 436 and 612 nm, respectively. The fluorescence spectra of **HTBT2** at various pH (Fig. 1b) showed that almost no fluorescence was observed at pH 9.30. However, a new emission band at $\sim$612 nm appeared with a gradual increase in intensity upon the decrease of pH from 9.30 to 6.40. Meanwhile, the orange-red fluorescence of solution enhanced gradually upon decreasing pH. Moreover, the lifetimes of **HTBT2** at various pH

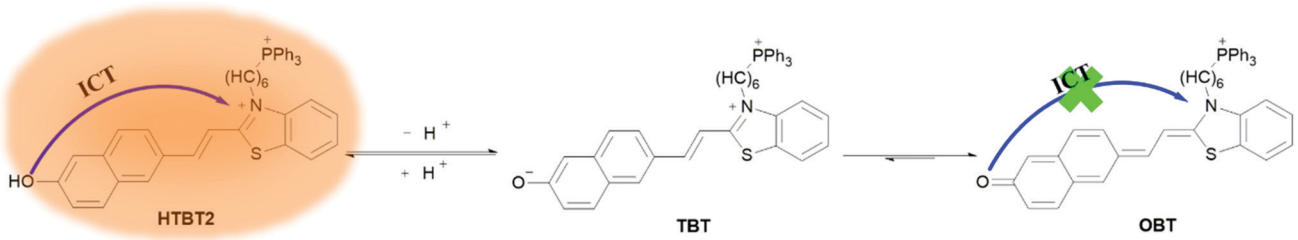


Scheme 1 Molecular structure of **HTBT2** in acidic and alkaline environments as well as its sensing mechanism for pH changes.

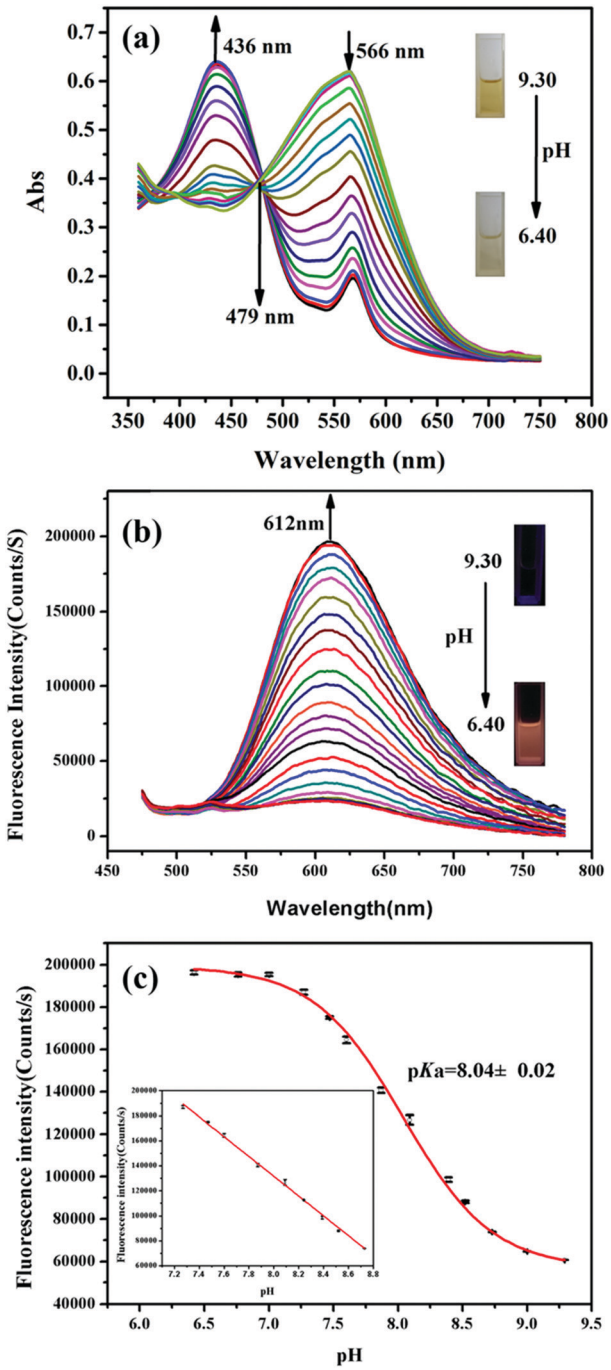


Fig. 1 (a) Absorption spectra changes of **HTBT2** (200 μM) upon decreasing the pH from 9.30 to 6.40. Inset: The solution colour change from yellow to yellow-green at pH 9.30 and 6.40, respectively. (b) The fluorescence spectra of **HTBT2** (10 μM) upon decreasing pH from 9.30 to 6.40 with an excitation at 436 nm. Inset: The photo of orange-red fluorescence of **HTBT2** at pH 6.40. (c) The pH-dependent fluorescence intensity at 612 nm was fitted *via* Boltzmann function. Inset: The good linearity between fluorescence intensity and pH in the range of pH 8.70–7.20.

values neared 7.01 μs (Table S1, ESI†). The fluorescence enhancement as a result of the formation of the protonated **HTBT2** improves the ICT process under acidic conditions. The fluorescence quantum yield of **HTBT2** was found to be 0.112 (DMSO) relative to Rhodamine 6G ($\Phi$ = 0.95 in water). It is worth noting that **HTBT2** showed a remarkably large Stokes shift of 176 nm, which could effectively reduce the excitation interference and then drastically improve the sensitivity of measurements.

To determine the p$K_a$ of **HTBT2**, Boltzmann function fitting of the pH-dependent fluorescence intensity at 612 nm was adapted. As shown in Fig. 1c, the p$K_a$ was found to be 8.04 ± 0.02, which was very close to the pH of the mitochondrial matrix (~8.0). There was a good linearity in the pH range of 8.70 to 7.20, based on the regression equation: $F$ = 764314.81192 − 79080.76184 × pH with $R^2$ of 0.9991. These results indicated that **HTBT2** could be potentially suitable for detecting mitochondrial pH variations.

### Mass spectra and $^1$H NMR spectra of HTBT2 assays with pH changes

To confirm the sensing mechanism of **HTBT2**, mass and $^1$H NMR titration experiments were implemented. The results of the mass spectra titration assays were displayed in Fig. S3 (ESI†), and the strong characteristic peak of **HTBT2** at 324.6273 and the negligible characteristic peak of **OBT** at 648.2699 were measured when the pH of the aqueous solution containing the probe was 6.40. The intensities of the peak at 314.6173 progressively decreased and the intensities of the peak at 648.2699 gradually increased as pH increased from 6.40 to 8.30, which was attributed to the conversion of **HTBT2** to **OBT** in the process. As shown in Fig. S4 (ESI†), the chemical shifts of $^1$H in **HTBT2** (in $d_6$-DMSO) at 10.02 ppm disappear step by step with pH increased from 6.40 to 9.30 in the $^1$H NMR spectra, which indicated that the mechanism of the probe sensing pH changes was achieved by the protonation and deprotonation of phenolic hydroxyl groups. Meanwhile, some of the proton resonances were clearly shifted upfield. Particularly, $^2$H vinyl proton significantly shifted upfield to 4.93 ppm. The upfield shift of those protons suggested that the generated naphthoxide *via* phenolic hydroxyl deprotonation was quickly transformed to naphthoquinone leading to the increase of electron density around those protons. The transformation was attributed to the fact that charge separation in the conjugate structure is extremely unstable. Thence, the above results indicated that deprotonation and protonation occurred on the phenolic hydroxyl of **HTBT2** and the generated **TBT** was quickly converted to **OBT**, providing a sensing mechanism for pH changes.

### Selectivity, photostability and reversibility of HTBT2

Considering the complexity of measured environments in live cells, the accuracy of pH measurement could be affected by various ions and biomolecules in live cells. Thus, the selectivity of **HTBT2** to $OH^-$ in the presence of other potential interfering species was studied at pH 6.40. The result depicted in Fig. S5 (ESI†) indicated that physiologically common metal cations, such as $K^+$, $Li^+$ and $Mg^{2+}$, along with other transition and heavy metal ions including $Co^{2+}$, $Hg^{2+}$, $Ni^{2+}$, $Ba^{2+}$ and $Cd^{2+}$, hardly caused noticeable emission intensity changes in the measurements.

 

Furthermore, some familiar anions (such as $Cl^-$, $Br^-$, $I^-$, $SO_4^{2-}$, $S_2O_3^{2-}$, $SO_3^{2-}$, $HS^-$, $NO_3^-$, $NO_2^-$, $Ac^-$, $HCO_3^-$ and $ClO_4^-$) and some other important substances (*e.g.* $H_2O_2$, HClO, $O_2^-$, NO, $ONOO^-$, L-glutathione, homocysteine and cysteine) exhibited negligible effect. These facts clearly indicated that **HTBT2** showed outstanding selectivity toward pH changes in the presence of background ions and biologically important species.

Subsequently, **HTBT2**'s stability was investigated *via* monitoring the fluorescence intensity change for 2 h in continuous light of 436 nm at room temperature. The fluorescence responses of **HTBT2** against time at pH 6.40 and 9.30 are shown in Fig. S6 (ESI†). As seen, the photostability **HTBT2** was very good at the measured pH range for 2 h.

The reversibility was one of the important prerequisites for real-time monitoring pH variations in actual biological samples. Subsequently, the pH value was modulated repeatedly between 6.40 and 9.30 by adding trace volume of HCl (1 M) and NaOH (1 M), and **HTBT2**'s fluorescence intensities were recorded at every moment. As clearly shown in Fig. S7 (ESI†), the response of **HTBT2** was fully reversible. Therefore, **HTBT2** is practically effective for use in tracking pH alterations in the real-time scale.

### Cytotoxicity assessment

To assess the cytotoxicity of the probe to live cells, the $IC_{50}$ value was determined by using the MTT assay.[33] The $IC_{50}$ value of **HTBT2** was obtained as 64.48 μM (Fig. S8, ESI†). This result clearly demonstrated that the probe showed low toxicity and is suitable for cell imaging experiments under the concentrations of 10 μM.

### Fluorescence imaging in live cells

Since mitochondria are the typical weakly alkaline organelles in cells, it is practically useful for **HTBT2** to sense the alkalinity if it can show subcellular localization of mitochondria. To assess the mitochondria staining ability of **HTBT2**, we conducted co-localization studies on SMMC-7721 cells with MitoTracker Green, a commercial mitochondria-specific green fluorescent dye. The bright red fluorescence images from **HTBT2** (Fig. 2a) merged well with those from MitoTracker Green (Fig. 2b–d), with a large mean Pearson's co-localization coefficient (A) of 0.92. Meanwhile, the changes in the intensity profile of **HTBT2** and MitoTracker Green in the linear regions tended toward synchronization (Fig. 2f). These results suggested that **HTBT2** selectively accumulated in mitochondria of SMMC-7721 cells, in addition to showing good cell membrane permeability (Fig. S9–S11, ESI†).

To explore the capability of **HTBT2** for imaging mitochondrial pH variations, the pH-dependent fluorescence images of **HTBT2** in live cells were investigated. As demonstrated in Fig. 3, the red fluorescence intensity in the SMMC-7721 cells gradually decreases upon increasing the pH from 7.0 to 9.0 and there is only little fluorescence detected at pH 9.00. These results meant that the **HTBT2** probe could effectively measure the mitochondrial pH in live cells. Moreover, the optical stability of the probe in the living cells at these pH values was also measured. As shown in Fig S12 (ESI†), the fluorescence intensities in cells decreases slightly (<5%) at

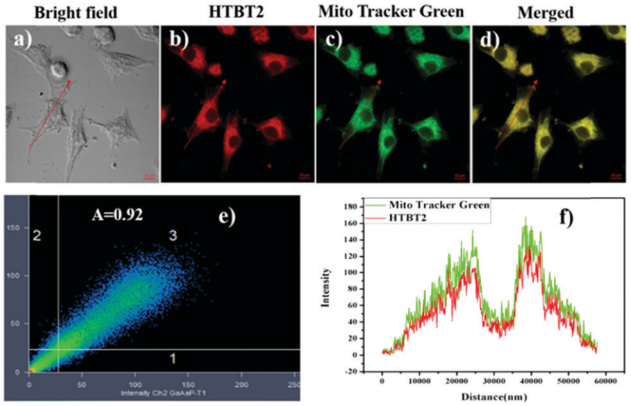


Fig. 2 The fluorescence imaging of SMMC-7721 cells co-labelled by 10 μM **HTBT2** (b) and 2 μM MitoTracker Green (c); (a) bright field imaging; (d) merged imaging; (e) the correlation of intensity distribution of **HTBT2** and MitoTracker Green ($A$ = 0.92); (f) intensity profile of intensity linear regions across the SMMC-7721 cells. The fluorescence imaging was implemented on an LSM-880+ Airyscan confocal laser scanning microscope with red channel ($E_x$ = 458 nm, $E_m$ = 560–660 nm) for **HTBT2**; green channel ($E_x$ = 488 nm, $E_m$ = 505 nm to 540 nm) for MitoTracker Green, respectively.

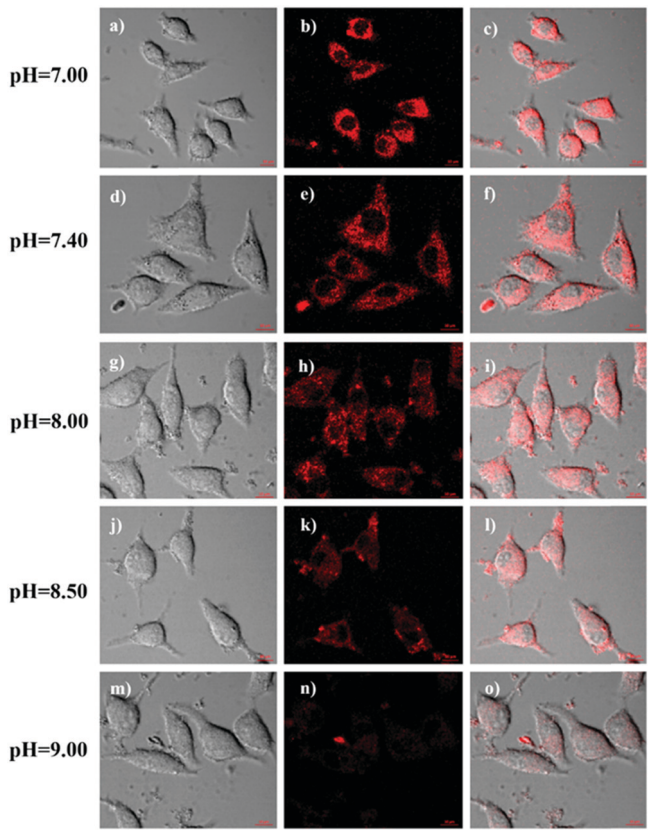


Fig. 3 (a–o) Fluorescence imaging of SMMC-7721 cells treated with 10 μM **HTBT2** at pH 7.00 (the first row), 7.40 (the second row), 8.00 (the third row), 8.50 (the fourth row) and 9.00 (the fifth row), respectively. The red channel imaging was collected at 560–660 nm ($E_x$ = 458 nm).

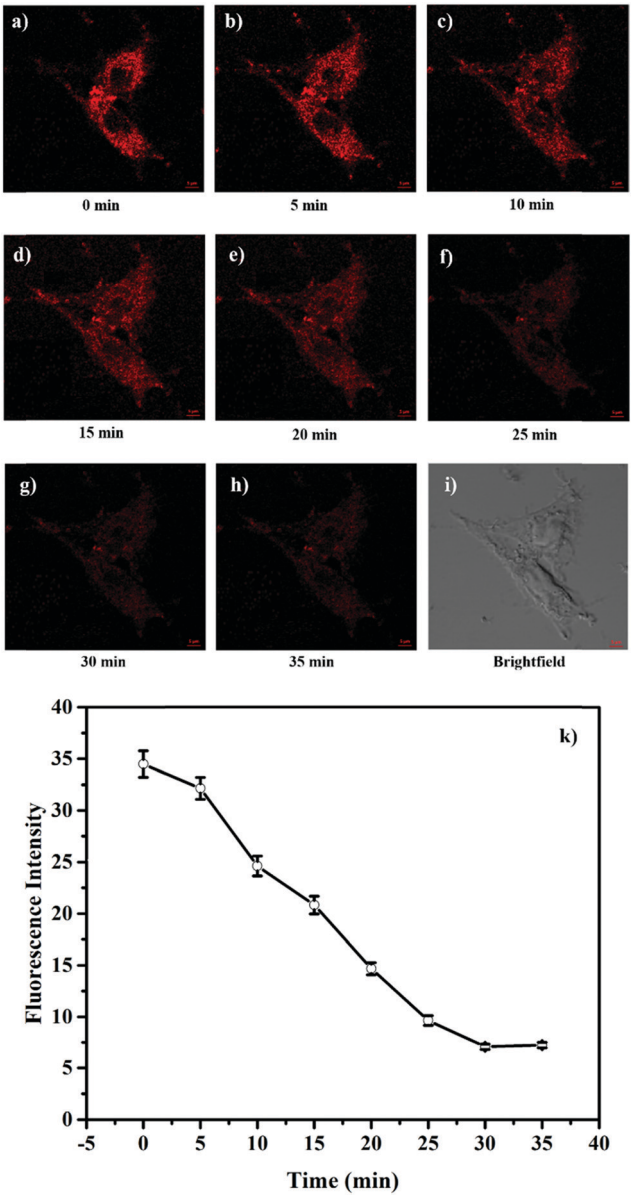


Fig. 4 (a–h) Fluorescence imaging of **HTBT2** (10 μM) in SMMC-7721 cells under different conditions with 5 mM $NH_4Cl$. (i) Brightfield images. The red channel imaging was collected at 568–650 nm ($E_x$ = 561 nm). (k) The mean fluorescence intensity changes of mitochondria after being treated with $NH_4Cl$ with time.

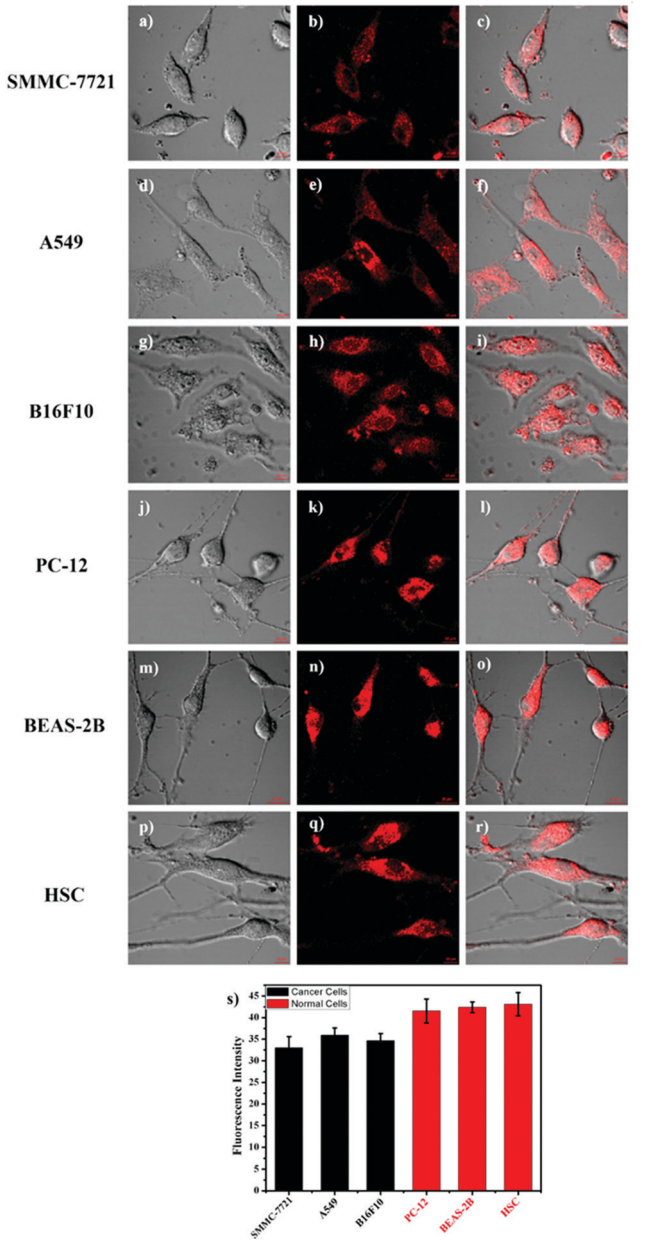


Fig. 5 (a–r) Fluorescence images of SMMC-7721 cells, A549 cells, B16F10 cells, PC-12 cells, BEAS-2B cells, and HSC cells stained with 10 μM **HTBT2**, respectively. (s) The fluorescence intensity plot of the above cell lines. The red channel imaging with 560–660 nm ($E_x$ = 458 nm) was collected. The thresholds were set to 0.4.

various pH. The phenomenon revealed that **HTBT2** possesses the potential to monitor mitochondrial pH changes in living cells for a long time.

The attractive mitochondria specificity and pH responsive ability of **HTBT2** urged us to further investigate the monitoring capability of $pH_{mito}$ changes in real time upon different stimulation. After incubation with 10 μM **HTBT2** for 10 min and washing three times with PBS, SMMC-7721 cells were further treated with 5 mM $NH_4Cl$, which could induce a dramatic increase in $pH_{mito}$ *via* neutralizing acid in the cells.[34] As depicted in Fig. 4 and Fig. S13 (ESI†), the fluorescence intensities in $NH_4Cl$-treated cells faded gradually within 25 min, and the changes of the fluorescence intensities from these cells after 30 min were negligible. This fact suggested that **HTBT2** exhibited a fast response to the alkalization in mitochondria.

It was reported that reactive oxygen species (ROS) as signalling molecules of apoptosis could be generated when the homeostasis of mitochondrial redox was destroyed, concomitant with variations in mitochondria pH.[35] In order to examine the relationship between mitochondrial pH and oxidative stress, SMMC-7721 cells stained with **HTBT2** were treated with 0.1 mM $H_2O_2$ and 1 mM NAC for 1 h, respectively. As depicted in Fig. S14 (ESI†),

 

compared with non-treated cells (the second row in Fig. S14d–f, ESI†), the mean fluorescence intensity (Fig. S14a–c, ESI†) in $H_2O_2$-treated cells obviously enhanced, unambiguously implying that the mitochondrial pH decreased. On the other hand, cells treated with NAC resulted in a slightly increased mitochondrial pH (Fig. S14g–i, ESI†). All of the above results clearly demonstrated that **HTBT2** could be employed for real-time detection of mitochondrial pH fluctuations in live cells.

It is well known that some diseases are closely related to mitochondrial pH abnormality, such as cancer.[8,10,11,36,37] To investigate the application and capability of **HTBT2** in differentiating the $pH_{mito}$ of cancer and normal cell lines by fluorescence imaging, three types of cancer cell lines including SMMC-7721 (human liver cancer cells); A549 (human alveolar cancer cells); and B16F10 (mouse melanoma cells) and three types of normal cell lines including PC-12 (rat neural cells); BEAS-2B (normal human alveolar cells); and HSC cells (human hematopoietic stem cells) were selected for the studies. Fig. 5 showed that the fluorescence intensities in the three normal cells lines were stronger than those of three cancer cells lines, consistently confirming that the $pH_{mito}$ in the cancer cells was higher than that in the normal cells.[38] Interesting, the fluorescence in cancer cells can be neglected when the thresholds were raised from 0.4 to 82 (Fig. S15, ESI†), while the fluorescence in normal cells can be observed easily. Furthermore, the results of dynamic assays shown that the time required for **HTBT2** to stain BEAS-2B cells ($\sim$12 min, Fig. S10, ESI†) and pc-12 cells ($\sim$13 min, Fig. S11, ESI†) was slightly shorter than that of SMMC-7721 cells ($\sim$18 min, Fig. S9, ESI†). Our results strongly supported that **HTBT2** showed a great clinical potential for differentiating cancer cells from normal cells.

## Conclusion

In summary, a benzothiazolium-based mitochondrial pH fluorescent probe **HTBT2** was facilely synthesized *via* Knoevenagel condensation reaction, for real-time visualization of mitochondrial pH fluctuations in live cells. **HTBT2** exhibited not only a significant Stokes shift of 176 nm, but also excellent selectivity toward slight pH changes, good reversibility and photostability, and low cytotoxicity. It is noted that the $pK_a$ value of the probe ($8.04 \pm 0.02$) matched $pH_{mito}$ ($\sim$8.0) well with a linear response range between pH 8.70 and 7.20. In addition to the excellent mitochondrial targeting ability, **HTBT2** showed an ability to detect and monitor mitochondrial pH fluctuations in live SMMC-7721 cells. Impressively, it was also successfully applied to differentiate the $pH_{mito}$ between cancer cell lines and normal cell lines. Therefore, **HTBT2** as the pH imaging probe offers practical potential to investigate physiological processes inside mitochondria.

## Conflicts of interest

There are no conflicts of interest to declare.

## Acknowledgements

The work was supported by the National Natural Science Foundation of China (No. 91843301, 21874087 and 81901814), the Key R&D project of Shanxi Province (201803D421031), Talents Project and General Research Fund (GRF) (HKBU 12301317) from the Research Grant Council of Hong Kong. We also appreciate Lanqi Huang, Di Xu, Tongxin Zhang and Wu Chun from Hong Kong Baptist University, Hong Kong for assisting with experiments.

## Notes and references

1 E. Guzel, S. Arlier, O. Guzeloglu-Kayisli, S. M. Tabak, T. Ekiz, N. Semerci, K. Larsen, F. Schatz, J. C. Lockwood and A. U. Kayisli, *Int. J. Mol. Sci.*, 2017, **18**, 792.
2 J. R. Casey, S. Grinstein and J. Orlowski, *Nat. Rev. Mol. Cell Biol.*, 2010, **11**, 50–61.
3 J.-T. Hou, W. X. Ren, K. Li, J. Seo, A. Sharma, X.-Q. Yu and J. S. Kim, *Chem. Soc. Rev.*, 2017, **46**, 2076–2090.
4 P. Paroutis, N. Touret and S. Grinstein, *Physiology*, 2004, **19**, 207–215.
5 X. Wang, L. Fan, Y. Wang, C. Zhang, W. Liang, S. Shuang and C. Dong, *J. Mater. Chem. B*, 2020, **8**, 1466–1471.
6 A. R. Sarkar, C. H. Heo, L. Xu, H. W. Lee, H. Y. Si, J. W. Byun and H. M. Kim, *Chem. Soc.*, 2016, **7**, 766–773.
7 L. P. Roma, J. Duprez, Hilton K. Takahashi, P. Gilon, A. Wiederkehr and J.-C. Jonas, *Biochem. J.*, 2012, **441**, 971.
8 A. H. V. Schapira, *Lancet*, 2006, **368**, 70–82.
9 H. Iwashita, S. Torii, N. Nagahora, M. Ishiyama, K. Shioji, K. Sasamoto, S. Shimizu and K. Okuma, *ACS Chem. Biol.*, 2017, **12**, 2546–2551.
10 M. H. Lee, N. Park, C. Yi, J. H. Han, J. H. Hong, K. P. Kim, D. H. Kang, J. L. Sessler, C. Kang and J. S. Kim, *J. Am. Chem. Soc.*, 2014, **136**, 14136–14142.
11 D. C. Wallace, *Nat. Rev. Cancer*, 2012, **12**, 685–698.
12 Y. Yue, F. Huo, S. Lee, C. Yin and J. Yoon, *Analyst*, 2017, **142**, 30–41.
13 P. Li, H. Xiao, Y. Cheng, W. Zhang, F. Huang, W. Zhang, H. Wang and B. Tang, *Chem. Commun.*, 2014, **50**, 7184–7187.
14 L. Gui, Z. Yuan, H. Kassaye, J. Zheng, Y. Yao, F. Wang, Q. He, Y. Shen, L. Liang and H. Chen, *Chem. Commun.*, 2018, **54**, 9675–9678.
15 M. J. Chang, K. Kim, K. S. Park, J. S. Kang, C. S. Lim, H. M. Kim, C. Kang and M. H. Lee, *Chem. Commun.*, 2018, **54**, 13531–13534.
16 X. Han, Z. Wang, Q. Cheng, X. Meng, D. Wei, Y. Zheng, J. Ding and H. Hou, *Dyes Pigm.*, 2017, **145**, 576–583.
17 S. Siriwibool, N. Kaekratoke, K. Chansaenpak, K. Siwawannapong, P. Panajapo, K. Sagarik, P. Noisa, R.-Y. Lai and A. Kamkaew, *Sci. Rep.*, 2020, **10**, 1283.
18 G. Li, B. Zhang, X. Song, Y. Xia, H. Yu, X. Zhang, Y. Xiao and Y. Song, *Sens. Actuators, B*, 2017, **253**, 58–68.
19 S. Qi, Q. Li, W. Liu, H. Ren, H. Zhang, J. Wu, J. Ge and P. Wang, *Spectrochim. Acta, Part A*, 2018, **204**, 590–597.

20 H. Yu, G. Li, B. Zhang, X. Zhang, Y. Xiao, J. Wang and Y. Song, *Dyes Pigm.*, 2016, **133**, 93–99.
21 D. Wang, Z. Wang, Y. Li, Y. Song, Y. Song, M. Zhang and H. Yu, *New J. Chem.*, 2018, **42**, 11102–11108.
22 X. Bi, Y. Wang, D. Wang, L. Liu, W. Zhu, J. Zhang and X. Zha, *RSC Adv.*, 2020, **10**, 26874–26879.
23 S. Xia, J. Wang, Y. Zhang, N. Whisman, J. Bi, T. E. Steenwinkel, S. Wan, J. Medford, M. Tajiri, R. L. Luck, T. Werner and H. Liu, *J. Mater. Chem. B*, 2020, **8**, 1603–1615.
24 M.-Y. Wu, K. Li, Y.-H. Liu, K.-K. Yu, Y.-M. Xie, X.-D. Zhou and X.-Q. Yu, *Biomaterials*, 2015, **53**, 669–678.
25 B. Lin, L. Fan, J. Ge, W. Zhang, C. Zhang, C. Dong and S. Shuang, *Analyst*, 2018, **143**, 5054–5060.
26 P. Wang, J. Huang and Y. Gu, *RSC Adv.*, 2016, **6**, 95708–95714.
27 L. Cao, Z. Zhao, T. Zhang, X. Guo, S. Wang, S. Li, Y. Li and G. Yang, *Chem. Commun.*, 2015, **51**, 17324–17327.
28 Y. Chen, C. Zhu, J. Cen, Y. Bai, W. He and Z. Guo, *Chem. Sci.*, 2015, **6**, 3187–3194.
29 L.-Q. Niu, J. Huang, Z.-J. Yan, Y.-H. Men, Y. Luo, X.-M. Zhou, J.-M. Wang and J.-H. Wang, *Spectrochim. Acta, Part A*, 2019, **207**, 123–131.
30 H. Wang, J. Hu, G. Yang, X. Zhang, R. Zhang, K. Uvdal, Z. Zhang, X. Wu and Z. Hu, *Sens. Actuators, B*, 2020, **320**, 128418.
31 X. Jiang, Z. Liu, Y. Yang, H. Li, X. Qi, W. X. Ren, M. Deng, M. Lü, J. Wu and S. Liang, *Spectrochim. Acta, Part A*, 2020, **224**, 117435.
32 B. Lin, L. Fan, Z. Ying, J. Ge, X. Wang, T. Zhang, C. Dong, S. Shuang and M. S. Wong, *Talanta*, 2020, **208**, 120279.
33 M. Li, J. Chou, K. W. King, J. Jing, D. Wei and L. Yang, *J. Lab. Autom.*, 2014, **20**, 32–45.
34 A. K. Ho, A. Ling and C. L. Chik, *J. Neurochem.*, 2000, **75**, 1845–1851.
35 K. Nomura, H. Imai, T. Koumura, M. Arai and Y. Nakagawa, *J. Biol. Chem.*, 1999, **274**, 29294–29302.
36 E. Carafoli and I. Roman, *Mol. Aspects Med.*, 1980, **3**, 295–429.
37 L. Galluzzi, N. Larochette, N. Zamzami and G. Kroemer, *Oncogene*, 2006, **25**, 4812–4830.
38 Y. Shi, S. K. Lim, Q. Liang, S. V. Iyer, H.-Y. Wang, Z. Wang, X. Xie, D. Sun, Y.-J. Chen, V. Tabar, P. Gutin, N. Williams, J. K. De Brabander and L. F. Parada, *Nature*, 2019, **567**, 341–346.

 